Supplementary Information (SI) for Energy Advances.

Supporting Information

A multi-metal (Fe, Cu, Zn) coordinated hollow porous dodecahedron nanocage catalyst reduces oxygen in Zn-air battery

Yanan Pan [a,1], Qi Yang [a, 1], Xiaoying Liu [a], Fan Qiu [a], Junjie Chen [a], Mengdie Yang [a], Yang Fan [a], Haiou Song [b], and Shupeng Zhang [a, *]

[a] *School of Chemistry and Chemical Engineering, Nanjing University of Science and Technology, Nanjing, 210094, PR China*

[b] *School of Environment, Nanjing Normal University, Nanjing, 210097, PR China*

[1] Y.N Pan and Q. Yang contributed equally to this work.

1. Experimental

1.1 Chemicals and Materials

KCl, Zinc nitrate hexahydrate, NaCl were purchased from Sinopharm Chemical Reagent Co., Ltd. Commercial 20 wt% Pt/C catalyst and (5%) Nafion solution were ordered from Sigma-Aldrich. Iron acetylacetonate, cupric nitrate, 2-methylimidazole, ethyl alcohol, methanol were obtained from Aladdin Chemistry Co., Ltd. All the materials were analytical reagents and were used without further purification. All aqueous solutions were prepared with secondary distilled water.

1.2 Electrochemical measurements

The electrocatalytic performance was evaluated on a CHI760E electrochemical analyzer (Chenhua Co., Shanghai, China). A conventional three-electrode cell was used, including a glassy carbon electrode (GCE) with a diameter of 4 mm was employed as the working electrode, a Pt wire as a counter electrode, and an Ag/AgCl (3M KCl) electrode as a reference electrode. And all of the potentials recorded in this part are given with respect to a reversible hydrogen electrode (RHE) by the formula E (RHE) = E(Ag/AgCl) + 0.0591pH + 0.197.

For the preparation of the catalyst, 4 mg of the catalyst was added to the water/ethanol/nafion (5:5:1) mixed solution (1.1 mL) to form a uniform ink dispersion. 5 μL of ink was dropped onto a GCE and then added 5 μL of ink after it dried. 4 mg of the 20% Pt/C was added to the water /nafion (10:1) mixed solution (1.1 mL). 10 μL of uniform ink was dropped onto a GCE and dried at room temperature. Cyclic voltammetry (CV) was carried out in the potential range from -0.8 to 0.2 V vs. AgCl at a scan rate of 50 mV/s. LSV was performed in same potential range as CV at various rotation rates (400–2400 rpm) in 0.1 M KOH. The durability test for methanol, methanol (1-3 M) was added to the 0.1 M KOH electrolyte around 1000 s, and the current was collected at a rotation speed of 1600 rpm at –0.1/-0.4 V (vs. Ag/AgCl). The accelerated degradation test (ADT) was carried out by testing the LSV curve before and after 5000 cycles from 0 V to -0.4 V at a scan rate of 100 mV/s. All tests were performed under N_2 or O_2-saturated conditions. Electrochemical impedance spectroscopy (EIS): For the collection of EIS spectra, the initial potential was -0.15 V (vs. Ag/AgCl). The amplitude was 0.005 V and the frequency was from 0.005 Hz to 1000 Hz.

The kinetic-limiting current (J_k) and the number of transferred electrons (n) can be calculated according to Koutecky-Levich (K-L) equation,

$$\frac{1}{J} = \frac{1}{J_k} + \frac{1}{J_d} = \frac{1}{J_k} + \frac{1}{B\varpi^{1/2}} \quad (1)$$

$$B = 0.2nF(D_0)^{2/3}\nu^{-1/6}C_0 \quad (2)$$

where j, j_d and ω are the detected current density, diffusion-limiting current density and angular velocity of electrode rotation, respectively, F is the Faraday constant (96,485 C/mol), D_0 is the diffusion coefficient (1.93×10^{-5} cm^2/s) of O_2 in 0.1 M KOH aqueous solution, v is the kinematic viscosity (0.011 cm^2/s) of the aqueous solution, C_0 is the bulk concentration of O_2 (1.2×10^{-6} mol/cm^3) in the electrolyte. [1].

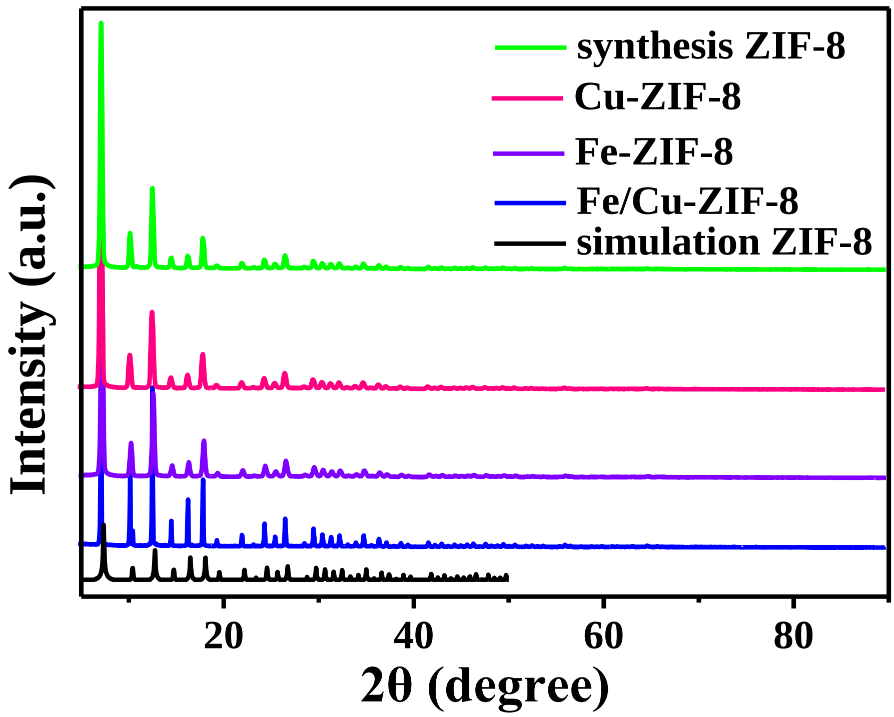

Figure S1. XRD spectra of Fe/Cu-ZIF-8, Fe-ZIF-8, Cu-ZIF-8 and ZIF-8.

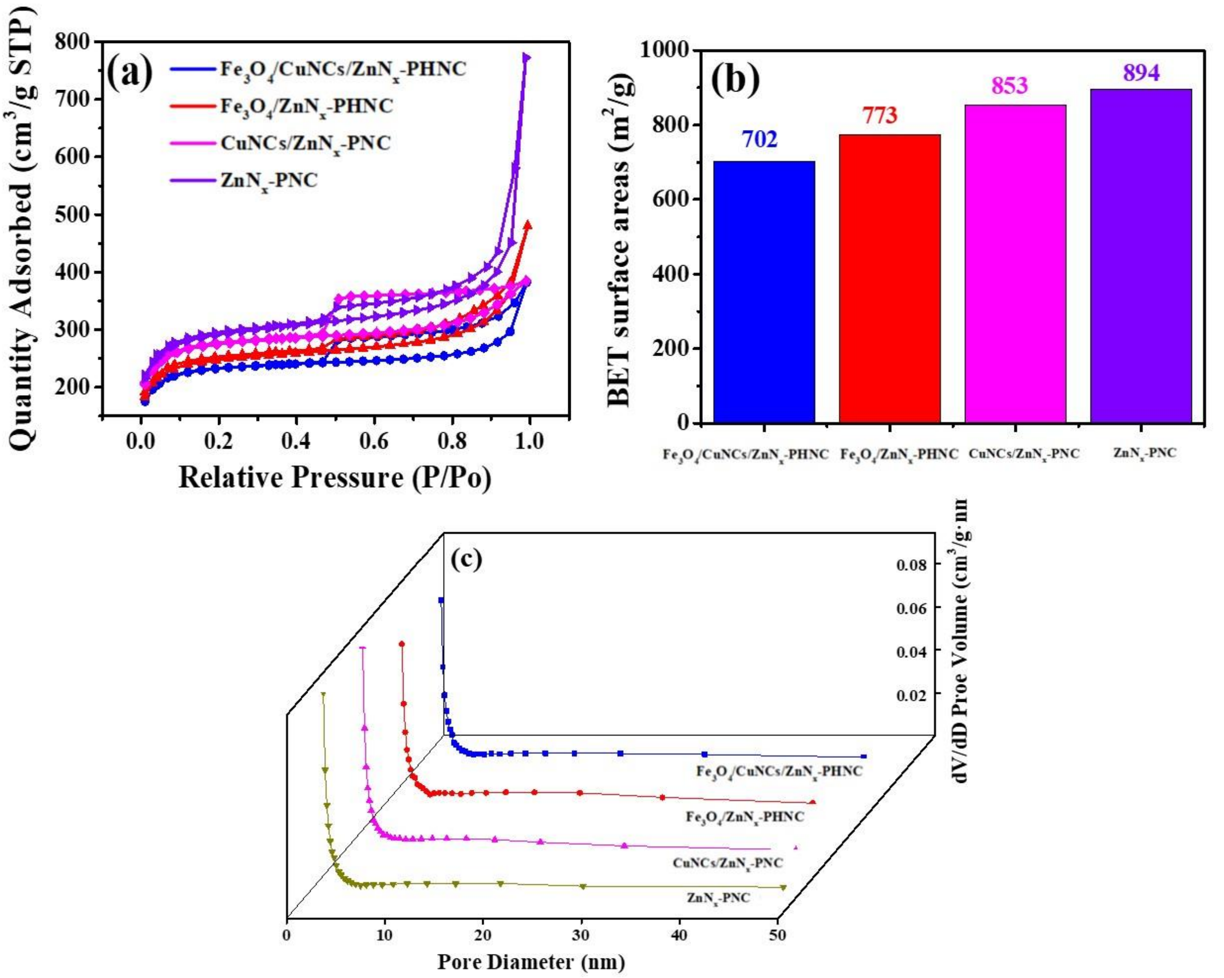

Figure S2 (a) Nitrogen adsorption and desorption isotherms of Fe_3O_4/CuNCs/ZnN_x-PHNC, Fe_3O_4/ZnN_x-PHNC, CuNCs/ZnN_x-PNC and ZnN_x-PNC; (b) BET histograms; (c) pore size distribution.

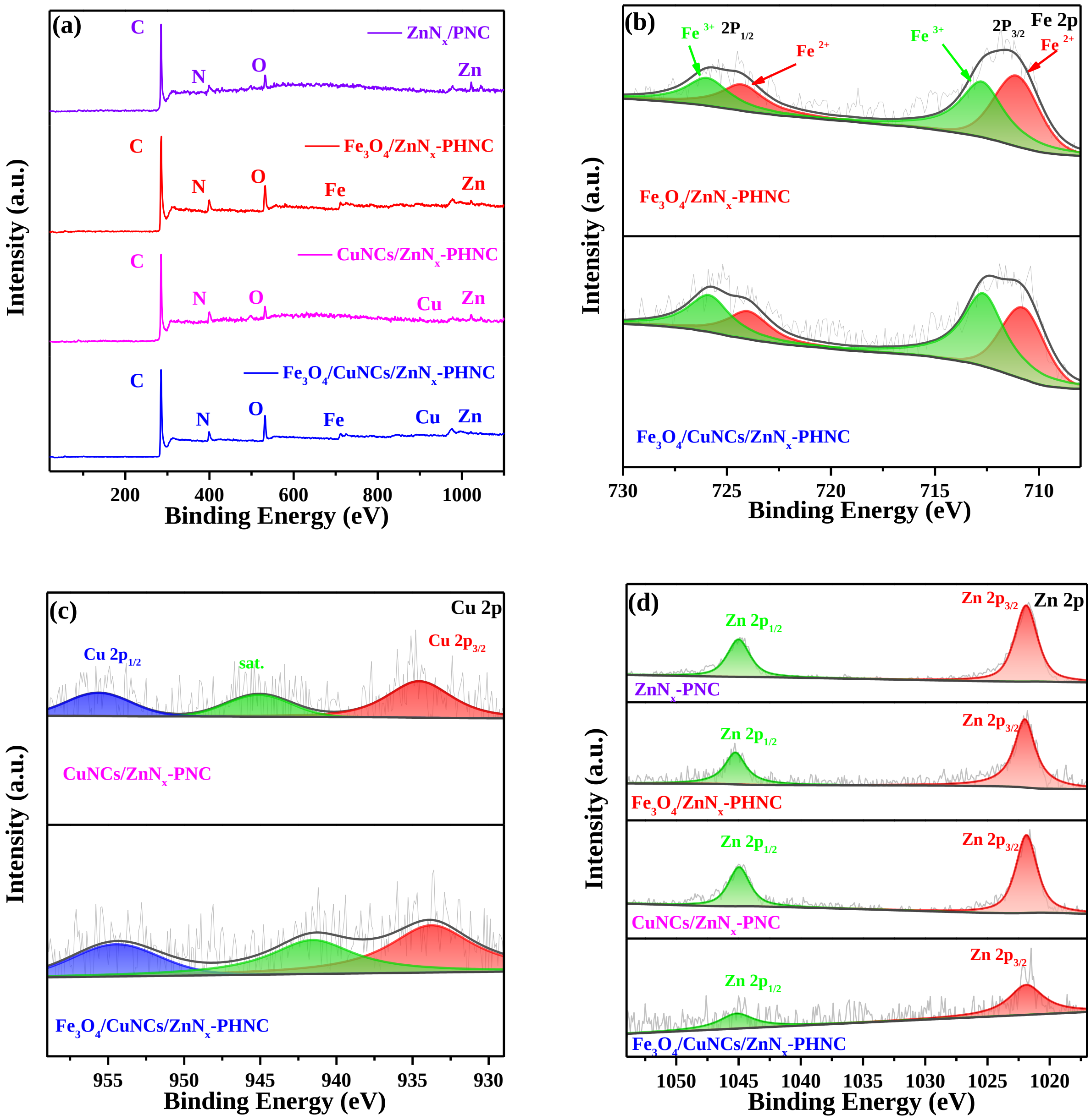

Figure S3 (a) XPS survey spectra; (b) XPS Fe 2p spectra; (c) XPS Cu 2p spectra and (d) XPS Zn 2p spectra.

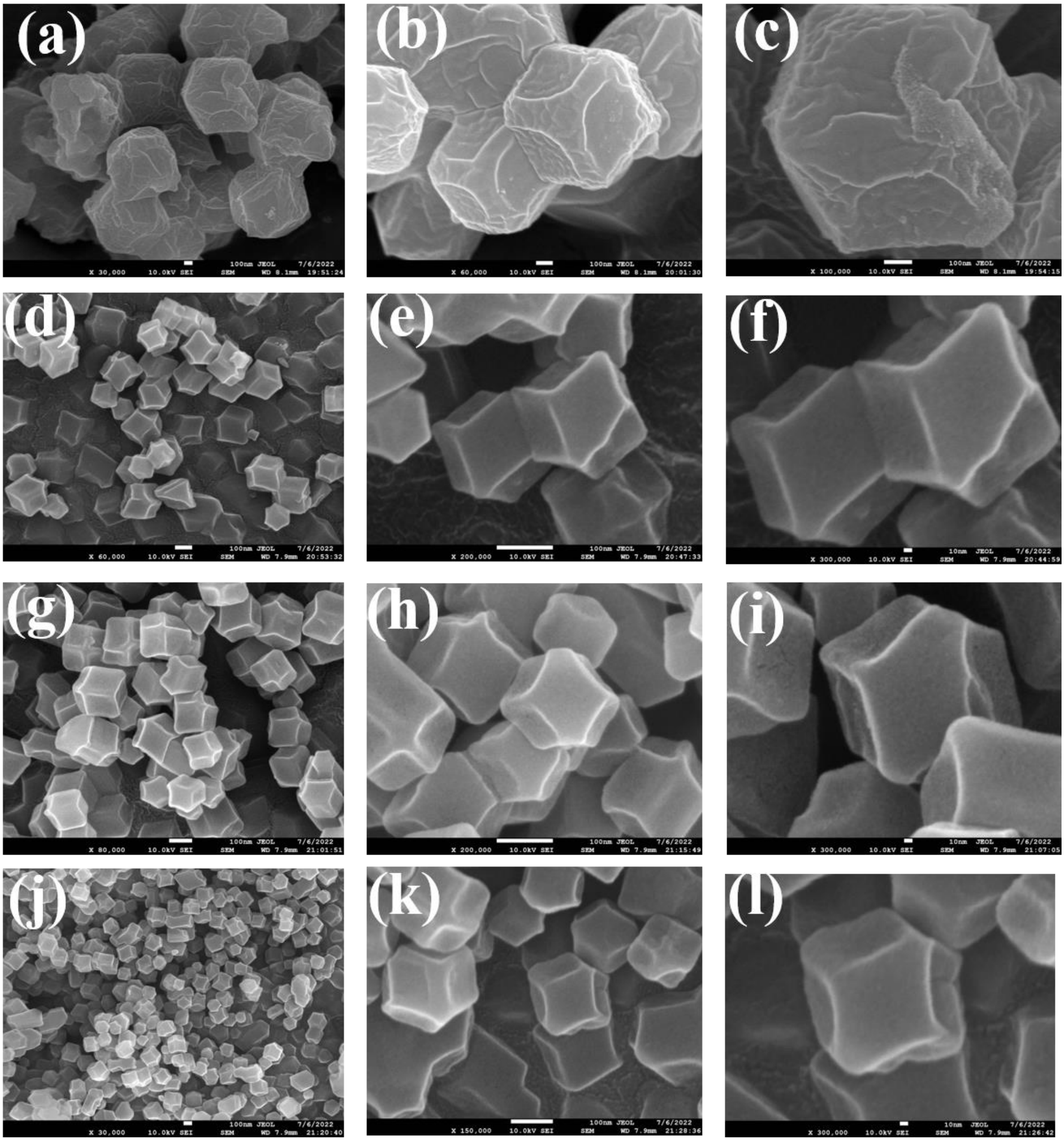

Figure S4. (a-c) SEM images of Fe-/Cu-ZIF-8 at different resolutions; (d-f) SEM images of Fe-ZIF-8 at different resolutions; (g-i) SEM images of Cu-ZIF-8 at different resolutions; (j-l) SEM images of ZIF-8 at different resolutions.

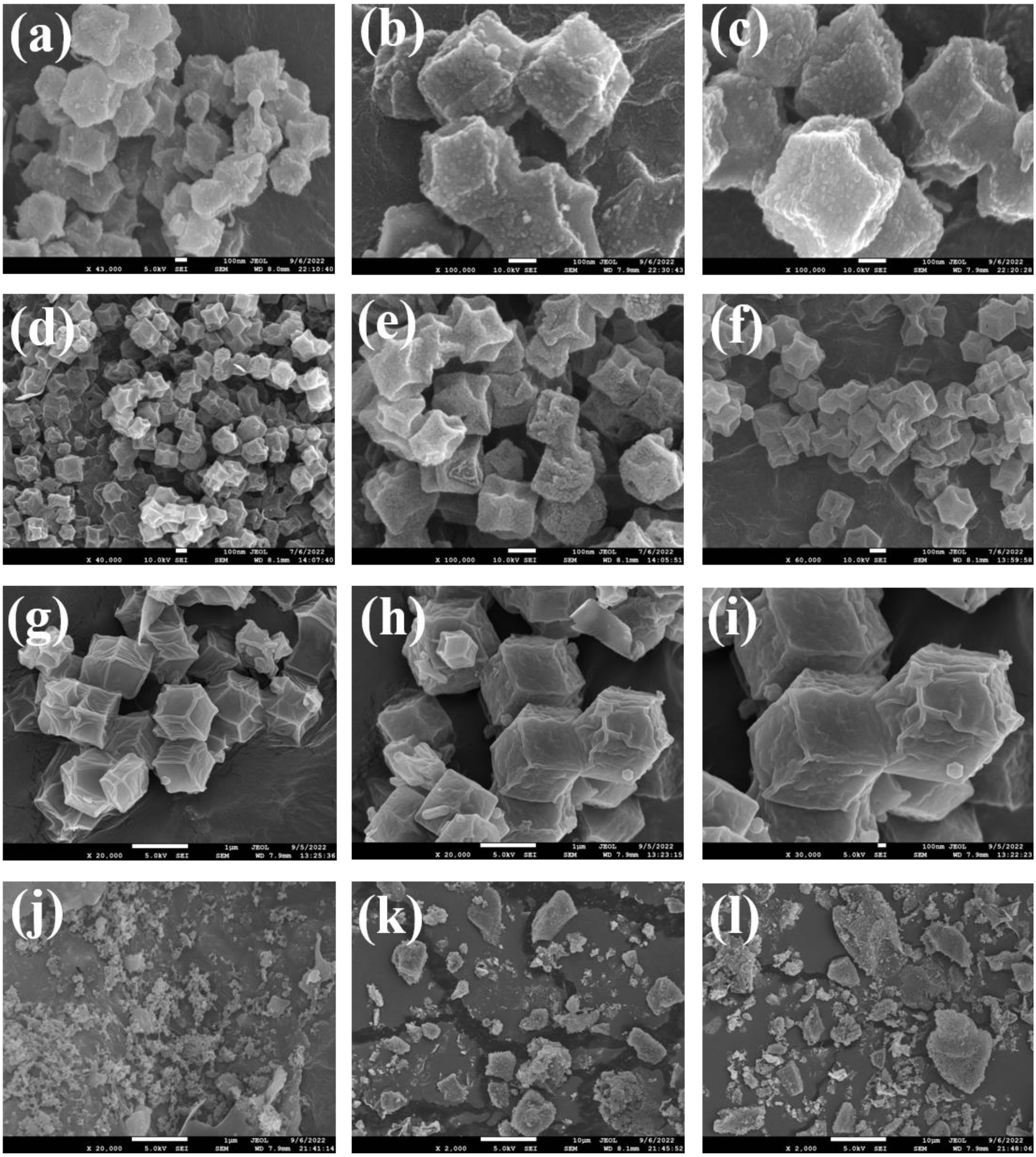

Figure S5 (a-c) SEM images of Fe_3O_4/CuNCs/ZnN_x-PHNC at different resolutions; (d-f) SEM images of Fe_3O_4/ZnN_x-PHNC at different resolutions; (g-i) SEM images of CuNCs/ZnN_x-PNC at different resolutions; (j-l) SEM images of ZnN_x-PNC at different resolutions.

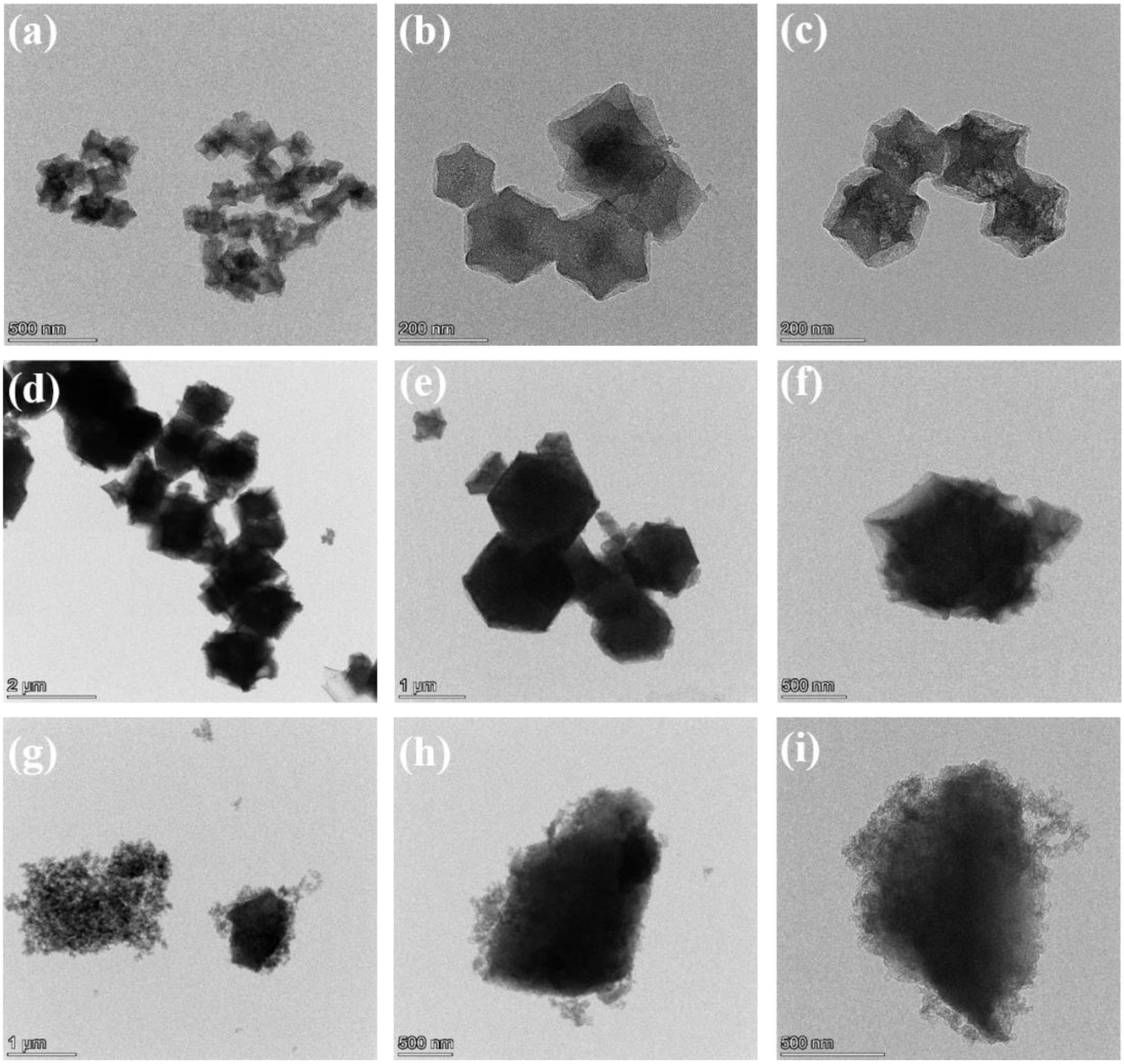

Figure S6. (a-c) TEM images of Fe_3O_4/ZnN_x-PHNC at different resolutions; (d-f) TEM images of CuNCs/ZnN_x-PNC at different resolutions; (g-i) TEM images of ZnN_x-PNC at different resolutions.

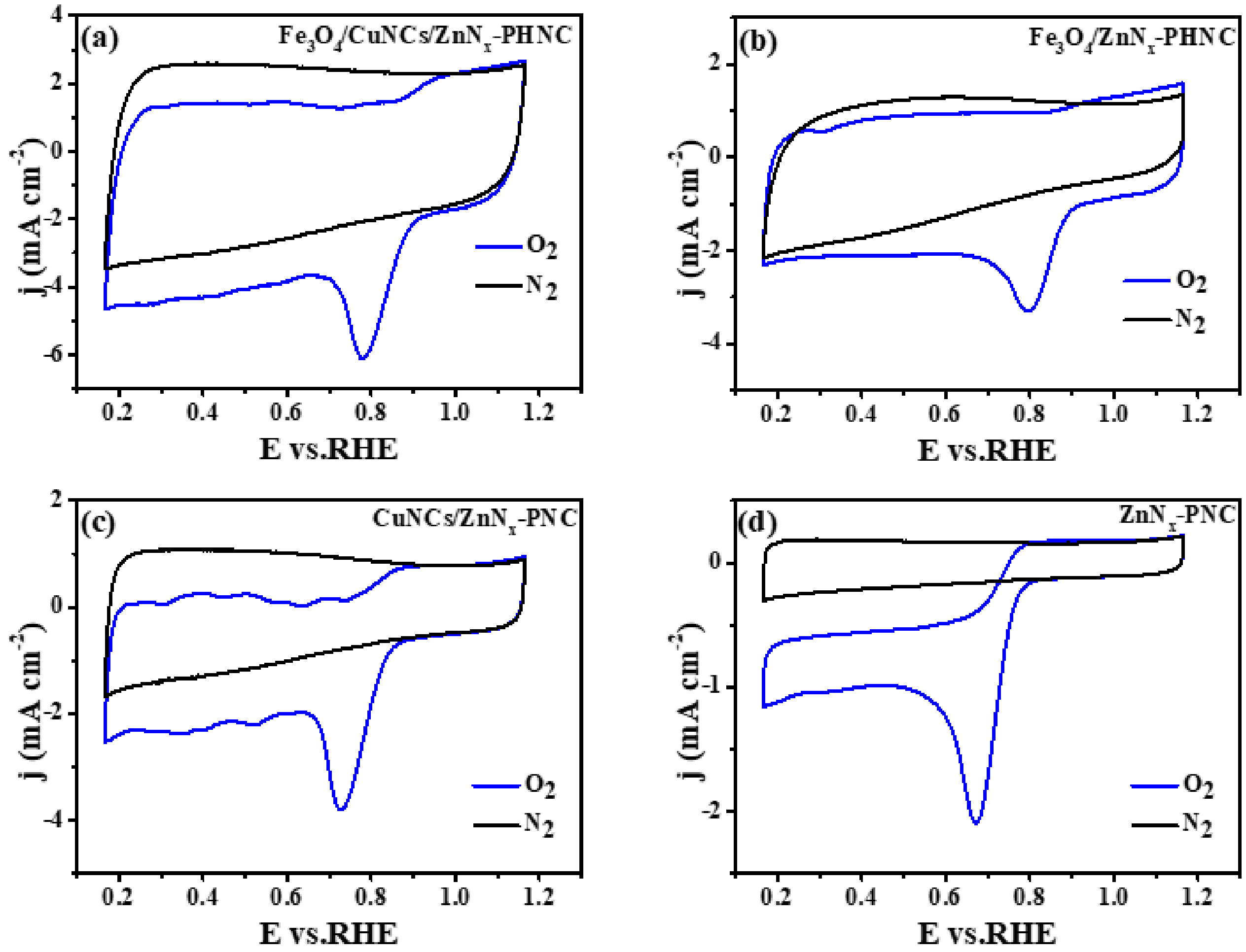

Figure S7. CV curves of (a) Fe_3O_4/CuNCs/ZnN_x-PHNC; (b) Fe_3O_4/ZnN_x-PHNC; (c) CuNCs/ZnN_x-PNC and (d) ZnN_x-PNC.

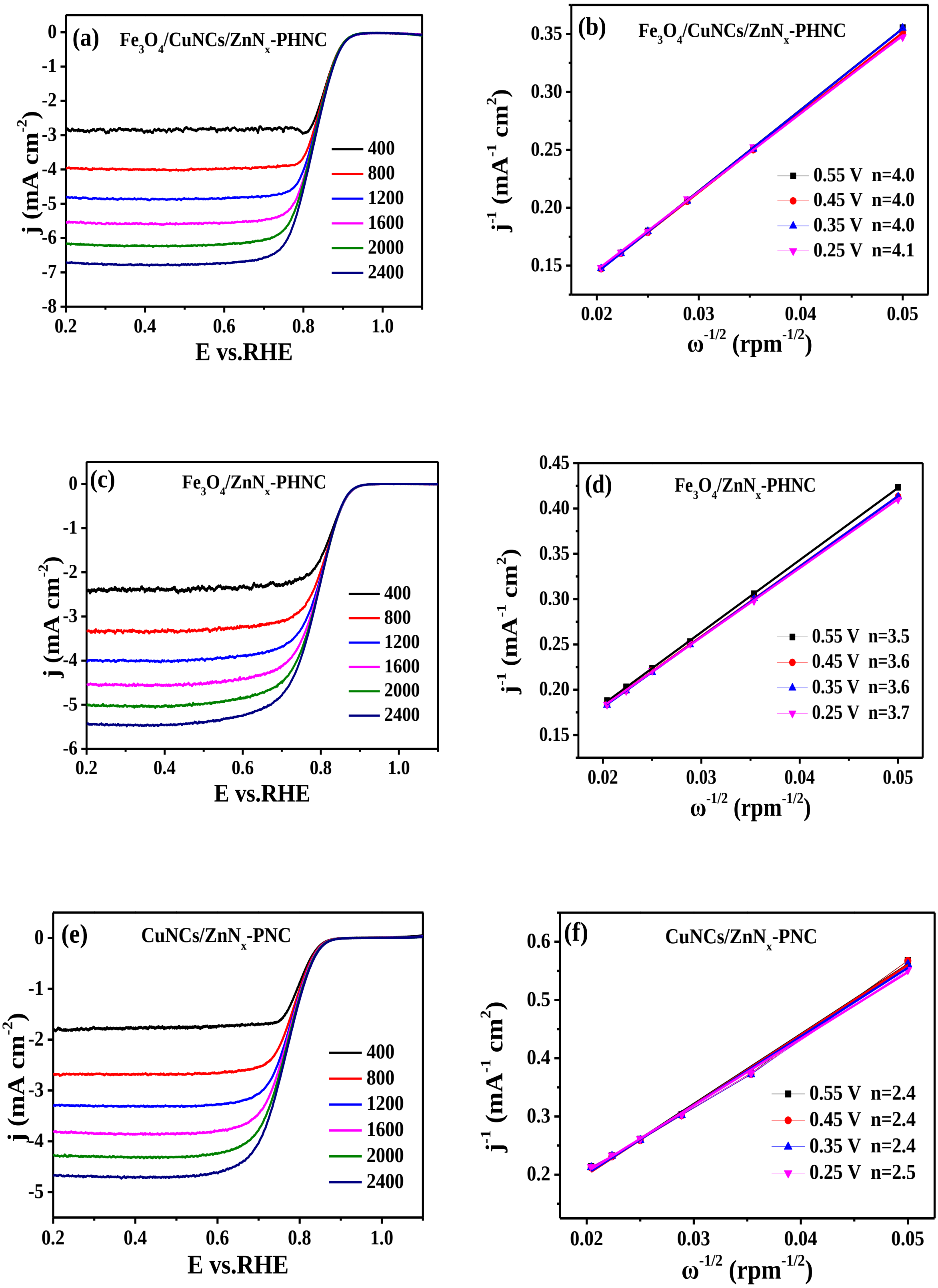

(a)
Fe3O4/CuNCs/ZnNx-PHNC
j (mA cm-2)
E vs.RHE
400
800
1200
1600
2000
2400
(b)
Fe3O4/CuNCs/ZnNx-PHNC
j-1 (mA-1 cm2)
ω-1/2 (rpm-1/2)
0.55 V n=4.0
0.45 V n=4.0
0.35 V n=4.0
0.25 V n=4.1
(c)
Fe3O4/ZnNx-PHNC
j (mA cm-2)
E vs.RHE
400
800
1200
1600
2000
2400
(d)
Fe3O4/ZnNx-PHNC
j-1 (mA-1 cm2)
ω-1/2 (rpm-1/2)
0.55 V n=3.5
0.45 V n=3.6
0.35 V n=3.6
0.25 V n=3.7
(e)
CuNCs/ZnNx-PNC
j (mA cm-2)
E vs.RHE
400
800
1200
1600
2000
2400
(f)
CuNCs/ZnNx-PNC
j-1 (mA-1 cm2)
ω-1/2 (rpm-1/2)
0.55 V n=2.4
0.45 V n=2.4
0.35 V n=2.4
0.25 V n=2.5

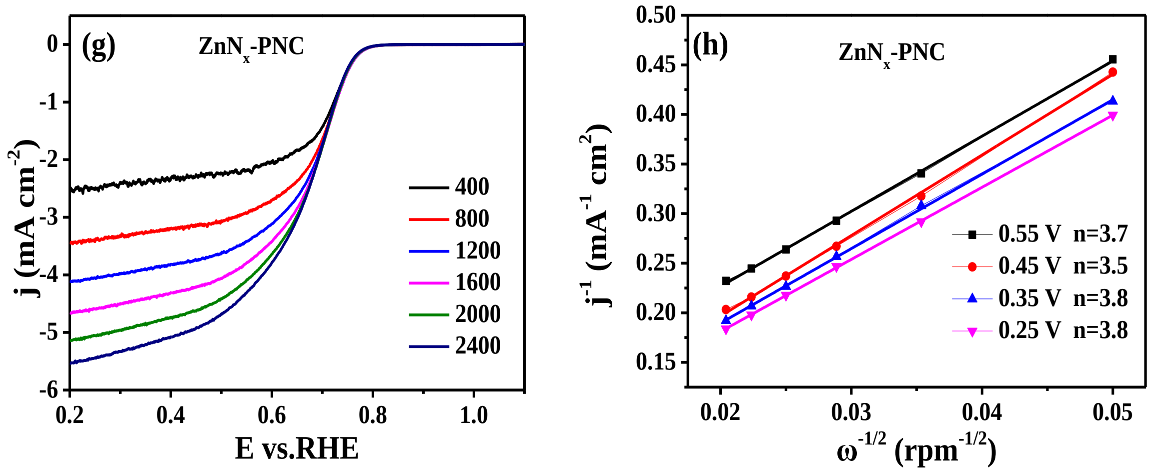

Figure S8 (a, b) Different rotational speeds and transferred electron number curves of Fe_3O_4/CuNCs/ZnN_x-PHNC; (c, d) Fe_3O_4/ZnN_x-PHNC; (e, f) CuNCs/ZnN_x-PNC and (g, h) ZnN_x-PNC.

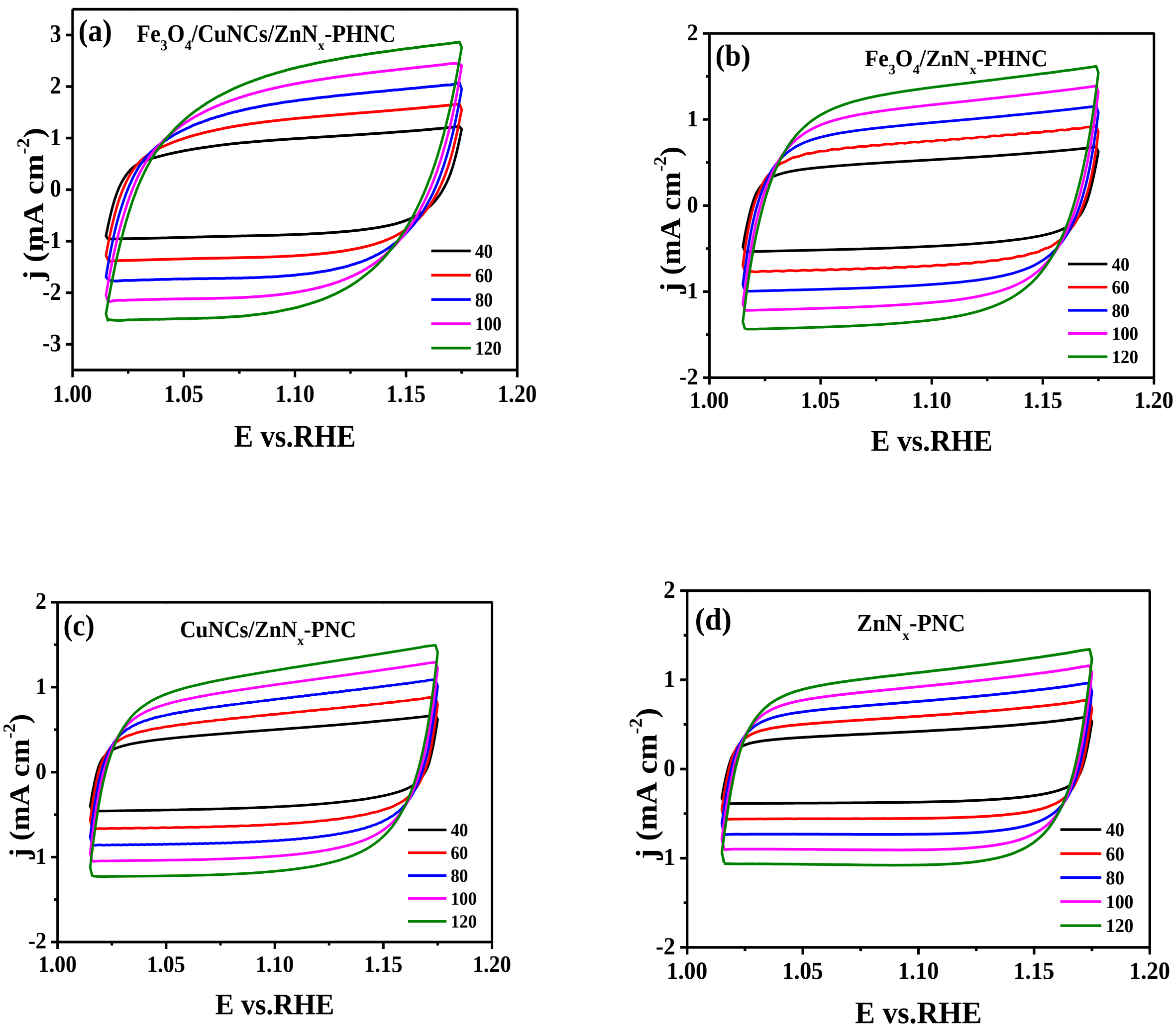

Figure S9. (a) Fe_3O_4/CuNCs/ZnN_x-PHNC; (b) Fe_3O_4/ZnN_x-PHNC; (c) CuNCs/ZnN_x-PNC and (d) CV plots of different scan rates of ZnN_x-PNC in 0.1 mol/L KOH at non-Faraday potentials from 1 V to 1.2 V (vs. RHE).

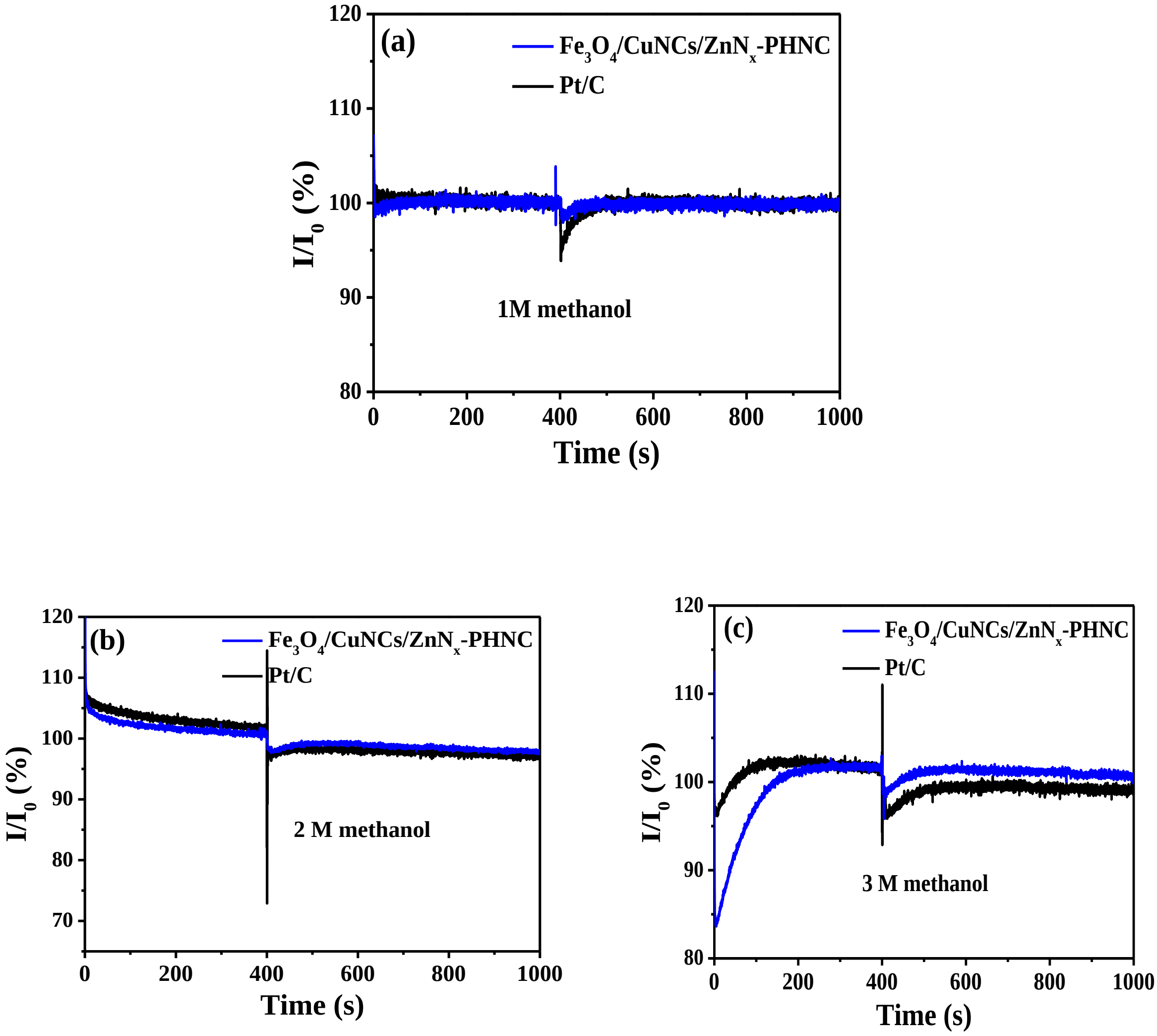

Figure S10. (a-c) Methanol resistance experiments of Fe_3O_4/CuNCs/ZnN_x-PHNC and Pt/C at different concentrations.

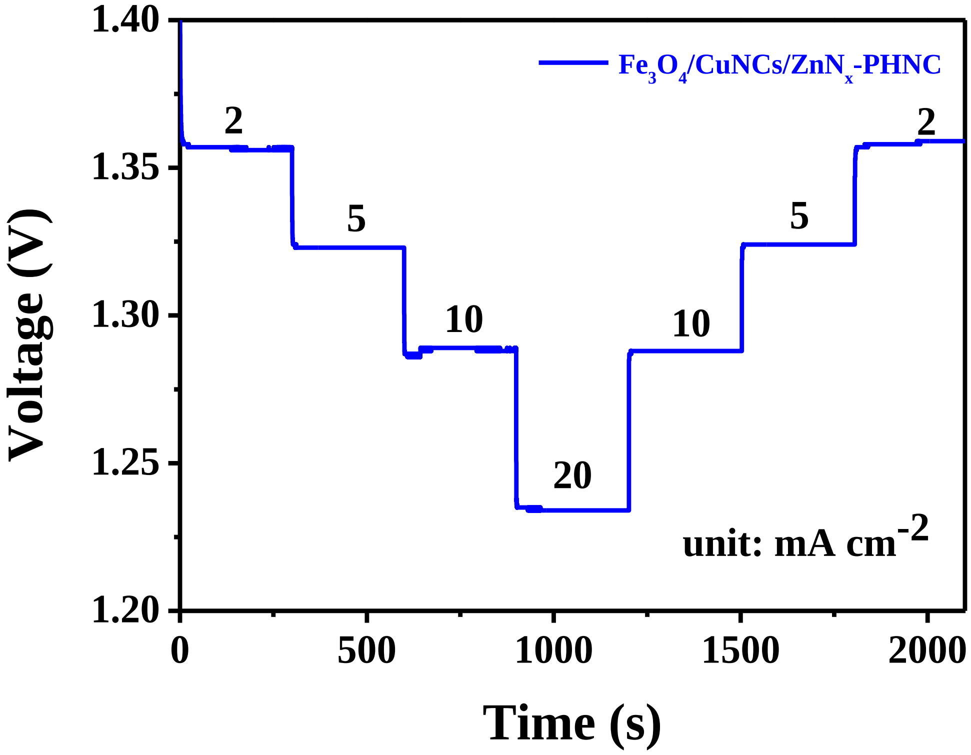

Figure S11 Multiplicative properties of Fe_3O_4/CuNCs/ZnN_x-PHNC-based ZAB.

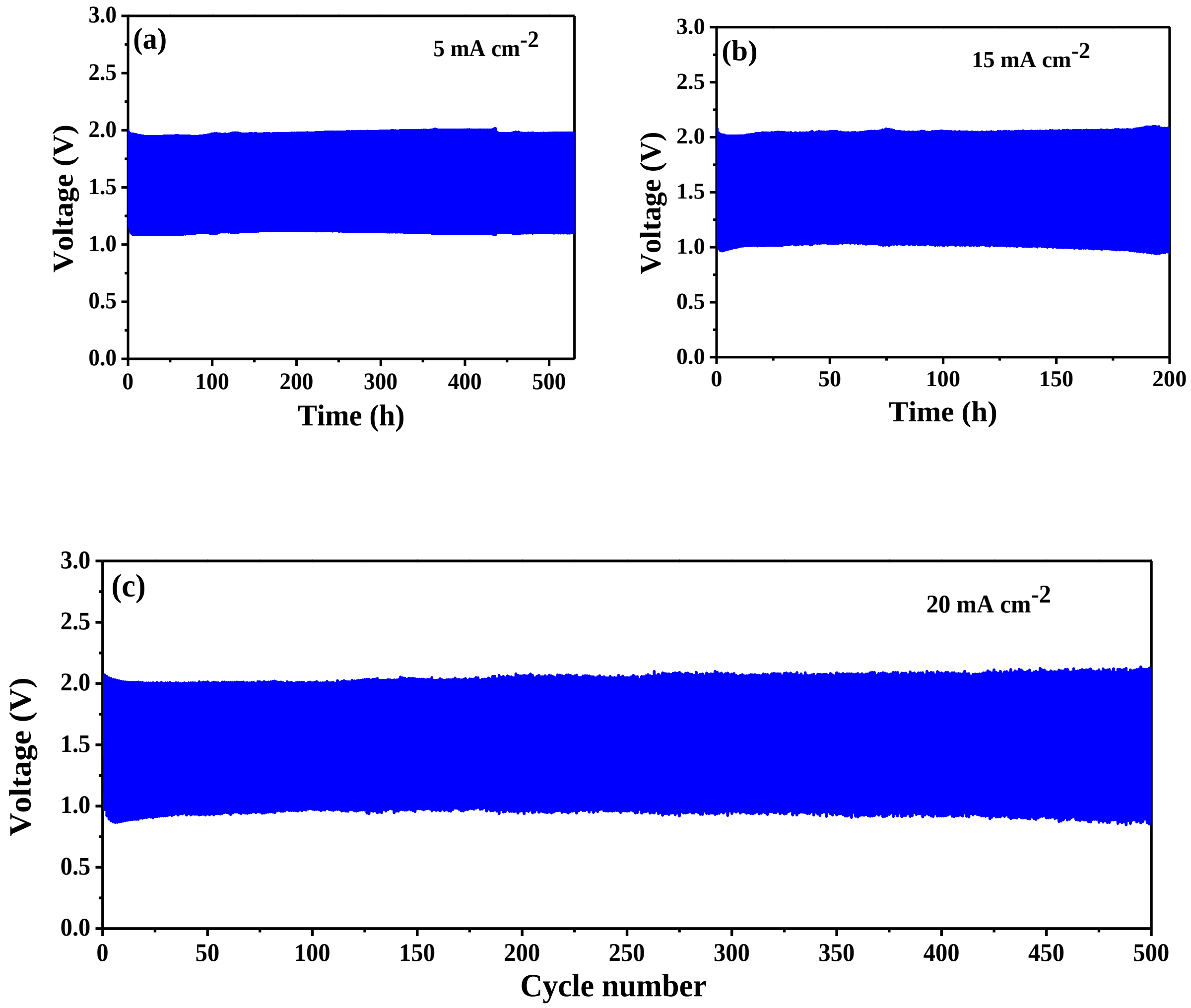

Figure S12. Charge/discharge curves of Fe_3O_4/CuNCs/ZnN_x-PHNC-based ZAB at different current densities.

Table S1. Raw Materials and the corresponding obtained materials.

	Zinc Nitrate Hexahydrate	**Dimethylimidazole**	**Iron Acetylacetonate**	**Copper Nitrate**
Fe_3O_4/CuNCs/ZnN_x-PHNC	√	√	√	√
Fe_3O_4/ZnN_x-PHNC	√	√	√	
CuNCs/ZnN_x-PNC	√	√		√
ZnN_x-PNC	√	√		

Table S2. BET and pore related data for different materials.

Samples	**BET (m^2/g)**	**t-Plot Micropore Area (m^2/g)**	**BJH Adsorption average pore diameter (nm)**	**BJH Adsorption cumulative volume of pores (cm^3/g)**
Fe_3O_4/CuNCs/ZnN_x-PHNC	**702**	**519.98**	**9.5**	**0.28**
Fe_3O_4/ZnN_x-PHNC	773	548.82	10.7	0.42
CuNCs/ZnN_x-PNC	853	627.22	6.0	0.23
ZnN_x-PNC	894	594.51	15.3	0.83

Table S3. XPS elemental analysis of ZnN_x-PNC, Fe_3O_4/ZnN_x -PHNC, CuNCS/ZnN_X-PNC and Fe_3O_4/ CuNCs/ZnN_x -PHNC.

Samples	C (atom %)	N (atom %)	O (atom %)	Zn (atom %)	Fe (atom %)	Cu (atom %)
ZnN_x-PNC	86.74	6.69	5.98	0.59	-	-
Fe_3O_4/ZnN_x -PHNC	84.02	6.11	8.92	0.19	0.73	-
CuNCs/ZnN_x-PNC	86.31	5.22	7.67	0.72	-	0.07
Fe_3O_4/CuNCs/ZnN_x-PHNC	**83.01**	**6.67**	**9.23**	**0.08**	**0.95**	**0.07**

Table S4. The relative contents of different C-sites derived from high-resolution XPS scans of C1s.

Samples	***sp*^{2} C=C** (atom %)	***sp*^{3} C-C** (atom %)	**C-N** (atom %)	**C-O** (atom %)
ZnN_x-PNC	39.49	32.65	16.99	10.87
Fe_3O_4/ZnN_x-PHNC	36.86	33.31	18.06	11.77
CuNCs/ZnN_x-PNC	42.31	31.59	16.55	9.55
Fe_3O_4/CuNCs/ZnN_x-PHNC	**42.09**	**29.35**	**21.82**	**6.73**

Table S5. The relative contents of different N-sites derived from high-resolution XPS scans of N1s.

Samples	**Pyridinic N** (atom %)	**Metal-N** (atom %)	**Pyrrolic N** (atom %)	**Graphitic N** (atom %)	**Oxidized N** (atom %)
ZnN_x-PNC	32.67	9.39	25.62	19.25	13.06
Fe_3O_4/ZnN_x-PHNC	30.05	17.37	26.42	18.22	7.94
CuNCs/ZnN_x-PNC	39.07	17.85	21.08	13.94	8.06
Fe_3O_4/CuNCs/ZnN_x-PHNC	**22.63**	**22.83**	**24.73**	**19.60**	**10.21**

Table S6. The relative contents of different O-sites derived from high-resolution XPS scans of O1s.

Samples	**Metal-O (atom %)**	**O_2^{2-}/O^- (atom %)**	**C-C=O (atom %)**	**H_2O (atom %)**
ZnN_x-PNC	10.47	21.63	31.33	36.57
Fe_3O_4/ZnN_x-PHNC	15.64	27.90	32.31	24.15
CuNCs/ZnN_x-PNC	7.98	28.08	26.02	37.92
Fe_3O_4/CuNCs/ZnN_x-PHNC	**20.71**	**33.75**	**22.90**	**22.64**

Table S7. Comparison of the ORR catalytic performance of **Fe_3O_4/CuNCs/ZnNx-PHNC** with recently reported materials.

Samples	*$E_{1/2}$ (V vs. RHE)*	*Tafel Slope (mV/dec)*	*Reference*
Fe_3O_4/CuNCs/ZnN_x-PHNC	***0.832***	***54***	***This work***
Fe-N/C-800	*0.809*	*-*	[2]
LD-Fe SAC	*0.81*	*74*	[3]
Fe-N-C SA/HCF	*0.802*	*-*	[4]
Fe–N–C/FeN	*0.81*	*80*	[5]
FeCo-1/NSC	*0.82*	*69.75*	[6]
NiFe@N-CFs	*0.82*	*58*	[7]
$Co_{0.5}Fe_{0.5}S$ @N-MC	*0.81*	*67*	[8]
Ni-N_4/GHSs/Fe-N_4	*0.83*	*55*	[9]
Fe_3C-FeSA@3DCN	*0.813*	*55*	[10]
FeS_2-CoS_2/NCFs	*0.81*	*55*	[11]

Fe/SNCFs-NH$_3$	*0.89*	*70.82*	[12]
Fe$_1$Co$_1$-CNF	*0.87*	*88*	[13]
FeNi@NCNT-CP	*0.85*	*79*	[14]
Fe,Ni-SAs/DNSC	*0.88*	*-*	[15]
Fe$_{20}$@N/HCSs	*0.850*	*58.7*	[16]
N-CNSP	*0.85*	*58*	[17]
A-SAC(Fe,Ni,Zn)/NC	*0.88*	*67*	[18]
Ni$_{66}$Fe$_{34}$-NC	*0.85*	*107*	[19]
ZOMC	*-*	*65.7*	[20]

Table S8. Impedance spectra fitting results for the ORR of Fe_3O_4/CuNCs/ZnN_x-PHNC, Fe_3O_4/ZnN_x-PHNC, CuNCs/ZnN_x-PNC and ZnN_x-PNC,

Samples	***R_s (Ω)***	***R_{ct} (Ω)***	***C_{dl} (10^{-4}Ω)***
Fe_3O_4/CuNCs/ZnN_x-PHNC	**2.06**	**52.74**	**2.1**
Fe_3O_4/ZnN_x-PHNC	2.18	40.23	1.6
CuNCs/ZnN_x-PNC	4.81	46.04	4.4
ZnN_x-PNC	5.13	53.56	6.9

Table S9. Performance comparison of advanced ZABs.

Catalyst	OCV(V)	Specific capacity ($mAh\ g^{-1}_{Zn}$)	Power density ($mW\ cm^{-2}$)	Stability	Reference
Fe_3O_4/CuNCs/ZnNx-PHNC	***1.45***	***818***	***162***	***500h@5 mA cm^{-2}***	***This work***
NiFe@N-CFs	*1.40*	*729*	*102*	*10h@10 mA cm^{-2}*	[7]
FeS_2-CoS_2/NCFs	*1.46*	*814*	*257*	*250h@10 mA cm^{-2}*	[11]
FeCo-N-C-700	*1.39*	*518*	*150*	*40h@5mA cm^{-2}*	[21]
NiFe-NC	1.44	765.5	140.1	*334h@20mA cm^{-2}*	[19]
Fe_3C-FeN/NC-2	1.41	745	166	*88h@10 mA cm^{-2}*	[22]
FeCo-NSC	1.51	782.1	152.8	*120h@20 mA cm^{-2}*	[23]
FeCu SACs/NC	1.48	741.9	153	*280 cycles@5mA cm^{-2}*	[24]

Fe–N/S-HPC	1.443	688	188.4	*240h@10mA cm^{-2}*	[25]
Fe-N/S-CNT-GR	-	912	123	*300h@10mA cm^{-2}*	[26]
NSC/Co_9S_8-200	1.47	741.8	176	*120h@20mA cm^{-2}*	[27]

Reference:

1. Nandan, R.; Nanda, K. K., A unique approach in designing resilient bi-functional nano-electrocatalysts based on ultrafine bimetallic nanoparticles dispersed in carbon nanospheres. *Journal of Materials Chemistry A* **2017,** *5* (21).

2. Lin, L.; Zhu, Q.; Xu, A.-W., Noble-Metal-Free Fe–N/C Catalyst for Highly Efficient Oxygen Reduction Reaction under Both Alkaline and Acidic Conditions. *Journal of the American Chemical Society* **2014,** *136* (31), 11027-11033.

3. Yang, J.; Wang, Z.; Huang, C.-X.; Zhang, Y.; Zhang, Q.; Chen, C.; Du, J.; Zhou, X.; Zhang, Y.; Zhou, H.; Wang, L.; Zheng, X.; Gu, L.; Yang, L.-M.; Wu, Y., Compressive Strain Modulation of Single Iron Sites on Helical Carbon Support Boosts Electrocatalytic Oxygen Reduction. *Angewandte Chemie International Edition* **2021,** *60* (42), 22722-22728.

4. Lei, J.; Liu, H.; Yin, D.; Zhou, L.; Liu, J.-A.; Chen, Q.; Cui, X.; He, R.; Duan, T.; Zhu, W., Boosting the Loading of Metal Single Atoms via a Bioconcentration Strategy. *Small* **2020,** *16* (10), 1905920.

5. Luo, X.; Wei, X.; Wang, H.; Gu, W.; Kaneko, T.; Yoshida, Y.; Zhao, X.; Zhu, C., Secondary-Atom-Doping Enables Robust Fe–N–C Single-Atom Catalysts with Enhanced Oxygen Reduction Reaction. *Nano-Micro Letters* **2020,** *12* (1), 163.

6. Chang, S.; Zhang, H.; Zhang, Z., FeCo alloy/N, S dual-doped carbon composite as a high-performance bifunctional catalyst in an advanced rechargeable zinc-air battery. *Journal of Energy Chemistry* **2021,** *56*, 64-71.

7. Niu, Y.; Teng, X.; Gong, S.; Chen, Z., A bimetallic alloy anchored on biomass-derived porous N-doped carbon fibers as a self-supporting bifunctional oxygen electrocatalyst for flexible Zn–air batteries. *Journal of Materials Chemistry A* **2020,** *8* (27), 13725-13734.

8. Shen, M.; Ruan, C.; Chen, Y.; Jiang, C.; Ai, K.; Lu, L., Covalent Entrapment of Cobalt–Iron Sulfides in N-Doped Mesoporous Carbon: Extraordinary Bifunctional Electrocatalysts for Oxygen

Reduction and Evolution Reactions. *ACS Applied Materials & Interfaces* **2015,** *7* (2), 1207-1218.

9. Chen, J.; Li, H.; Fan, C.; Meng, Q.; Tang, Y.; Qiu, X.; Fu, G.; Ma, T., Dual Single-Atomic Ni-N4 and Fe-N4 Sites Constructing Janus Hollow Graphene for Selective Oxygen Electrocatalysis. *Advanced Materials* **2020,** *32* (30), 2003134.

10. Yang, Q.; Liu, R.; Pan, Y.; Cao, Z.; Zuo, J.; Qiu, F.; Yu, J.; Song, H.; Ye, Z.; Zhang, S., Ultrahigh-Loaded Fe Single Atoms and Fe(3)C Nanoparticle Catalysts as Air Cathodes for High-Performance Zn-Air Batteries. *ACS Appl Mater Interfaces* **2023,** *15* (4), 5720-5731.

11. Shi, X.; He, B.; Zhao, L.; Gong, Y.; Wang, R.; Wang, H., FeS2–CoS2 incorporated into nitrogen-doped carbon nanofibers to boost oxygen electrocatalysis for durable rechargeable Zn-air batteries. *Journal of Power Sources* **2021,** *482*, 228955.

12. Yang, L.; Zhang, X.; Yu, L.; Hou, J.; Zhou, Z.; Lv, R., Atomic Fe–N4/C in Flexible Carbon Fiber Membrane as Binder-Free Air Cathode for Zn–Air Batteries with Stable Cycling over 1000 h. *Advanced Materials* **2022,** *34* (5), 2105410.

13. Wang, Y.; Li, Z.; Zhang, P.; Pan, Y.; Zhang, Y.; Cai, Q.; Silva, S. R. P.; Liu, J.; Zhang, G.; Sun, X.; Yan, Z., Flexible carbon nanofiber film with diatomic Fe-Co sites for efficient oxygen reduction and evolution reactions in wearable zinc-air batteries. *Nano Energy* **2021,** *87*, 106147.

14. Zheng, X.; Cao, X.; Zeng, K.; Yan, J.; Sun, Z.; Rümmeli, M. H.; Yang, R., A Self-Jet Vapor-Phase Growth of 3D FeNi@NCNT Clusters as Efficient Oxygen Electrocatalysts for Zinc-Air Batteries. *Small* **2021,** *17* (4), 2006183.

15. Zhang, X.; Li, Y.; Jiang, M.; Wei, J.; Ding, X.; Zhu, C.; He, H.; Lai, H.; Shi, J., Engineering the coordination environment in atomic Fe/Ni dual-sites for efficient oxygen electrocatalysis in Zn-air and Mg-air batteries. *Chemical Engineering Journal* **2021,** *426*, 130758.

16. Wang, B.; Ye, Y.; Xu, L.; Quan, Y.; Wei, W.; Zhu, W.; Li, H.; Xia, J., Space-Confined Yolk-Shell Construction of Fe3O4 Nanoparticles Inside N-Doped Hollow Mesoporous Carbon Spheres as Bifunctional Electrocatalysts for Long-Term Rechargeable Zinc–Air Batteries. *Advanced Functional*

Materials **2020,** *30* (51), 2005834.

17. Zong, L.; Wu, W.; Liu, S.; Yin, H.; Chen, Y.; Liu, C.; Fan, K.; Zhao, X.; Chen, X.; Wang, F.; Yang, Y.; Wang, L.; Feng, S., Metal-free, active nitrogen-enriched, efficient bifunctional oxygen electrocatalyst for ultrastable zinc-air batteries. *Energy Storage Materials* **2020,** *27*, 514-521.

18. Tsai, J.-E.; Hong, W.-X.; Pourzolfaghar, H.; Wang, W.-H.; Li, Y.-Y., A Fe-Ni-Zn triple single-atom catalyst for efficient oxygen reduction and oxygen evolution reaction in rechargeable Zn-air batteries. *Chemical Engineering Journal* **2023,** *460*, 141868.

19. Ma, M.; Kumar, A.; Wang, D.; Wang, Y.; Jia, Y.; Zhang, Y.; Zhang, G.; Yan, Z.; Sun, X., Boosting the bifunctional oxygen electrocatalytic performance of atomically dispersed Fe site via atomic Ni neighboring. *Applied Catalysis B: Environmental* **2020,** *274*, 119091.

20. Douka, A. I.; Xu, Y.; Yang, H.; Zaman, S.; Yan, Y.; Liu, H.; Salam, M. A.; Xia, B. Y., A Zeolitic-Imidazole Frameworks-Derived Interconnected Macroporous Carbon Matrix for Efficient Oxygen Electrocatalysis in Rechargeable Zinc–Air Batteries. *Advanced Materials* **2020,** *32* (28), 2002170.

21. Duan, X.; Ren, S.; Pan, N.; Zhang, M.; Zheng, H., MOF-derived Fe,Co@N–C bifunctional oxygen electrocatalysts for Zn–air batteries. *Journal of Materials Chemistry A* **2020,** *8* (18), 9355-9363.

22. Zhou, F.; Yu‡, P.; Sun, F.; Zhang, G.; Liu, X.; Wang, L., The cooperation of Fe_3C nanoparticles with isolated single iron atoms to boost the oxygen reduction reaction for Zn–air batteries. *Journal of Materials Chemistry A* **2021,** *9* (11), 6831-6840.

23. Wu, Y.; Ye, C.; Yu, L.; Liu, Y.; Huang, J.; Bi, J.; Xue, L.; Sun, J.; Yang, J.; Zhang, W.; Wang, X.; Xiong, P.; Zhu, J., Soft template-directed interlayer confinement synthesis of a Fe-Co dual single-atom catalyst for Zn-air batteries. *Energy Storage Materials* **2022,** *45*, 805-813.

24. Liu, H.; Jiang, L.; Wang, Y.; Wang, X.; Khan, J.; Zhu, Y.; Xiao, J.; Li, L.; Han, L., Boosting oxygen reduction with coexistence of single-atomic Fe and Cu sites decorated nitrogen-doped porous carbon. *Chemical Engineering Journal* **2023,** *452*.

25. Wang, M.; Du, X.; Zhang, M.; Su, K.; Li, Z., From S-rich polyphenylene sulfide to honeycomb-

like porous carbon with ultrahigh specific surface area as bifunctional electrocatalysts for rechargeable Zn-air batteries. *Carbon* **2022,** *198*, 264-274.

26. Noh, W. Y.; Mun, J.; Lee, Y.; Kim, E. M.; Kim, Y. K.; Kim, K. Y.; Jeong, H. Y.; Lee, J. H.; Song, H.-K.; Lee, G.; Lee, J. S., Molecularly Engineered Carbon Platform To Anchor Edge-Hosted Single-Atomic M–N/C (M = Fe, Co, Ni, Cu) Electrocatalysts of Outstanding Durability. *ACS Catalysis* **2022,** *12* (13), 7994-8006.

27. Zheng, Q.; Xiong, Y.; Tang, K.; Wu, M.; Hu, H.; Zhou, T.; Wu, Y.; Cao, Z.; Sun, J.; Yu, X.; Wu, C., Modulation of pore-size in N, S-codoped carbon/Co9S8 hybrid for a stronger O2 affinity toward rechargable zinc-air battery. *Nano Energy* **2022,** *92*.